Inorganic Chemistry

Article

pubs.acs.org/IC

Synthesis, Characterization, and Linkage Isomerism in Mononuclear Ruthenium Complexes Containing the New Pyrazolate-Based Ligand Hpbl

Laia Francàs,[†,§] Rosa M. González-Gil,[§] Albert Poater,[‡] Xavier Fontrodona,[‡] Jordi García-Antón,[§] Xavier Sala,*[,§] Lluís Escriche,*[,§] and Antoni Llobet*[,†,§]

[†]Institute of Chemical Research of Catalonia (ICIQ), Avingunda Països Catalans 16, E-43007 Tarragona, Spain

[‡]Serveis Tècnics de Recerca, Institut de Química Computacional i Catàlisi and Departament de Química, Universitat de Girona, Campus de Montilivi, E-17071 Girona, Spain

[§]Departament de Química, Universitat Autònoma de Barcelona, Cerdanyola del Vallès, 08193, Barcelona, Spain

Supporting Information

ABSTRACT: A new tetradentate dinucleating ligand [1,1′-(4-methyl-1*H*-pyrazole-3,5-diyl)bis(1-(pyridin-2-yl)ethanol)] (Hpbl) containing an O/N mixed donor set of atoms has been synthesized and characterized by analytical and spectroscopic techniques. The Ru−Cl and Ru−aqua complexes containing this ligand of general formula $[Ru^{II}X(Hpbl)(trpy)]^{y+}$ (trpy = 2,2′:6′,2″-terpyridine; X = Cl, y = 1; X = H_2O, y = 2) have been prepared and thoroughly characterized by spectroscopic and electrochemical techniques. The Ru−aqua complex **2** undergoes N → O linkage isomerization as observed electrochemically, and the related thermodynamic and kinetic parameters are extracted from cyclic voltammetry experiments together with DIGISIM, a CV simulation package. Under basic conditions an additional isomer is observed where the pyrazolyl group in the Hpbl ligand is replaced by the geminal pyridyl group. Further structural and electronic characterization of all the isomers has been carried out by means of DFT calculations.

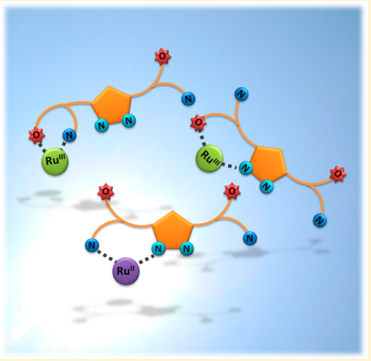

INTRODUCTION

Linkage isomerism has been used to build memory devices at the molecular level, which could provide the basis for the development of molecular electronics.[1] Transition metal complexes with ambidentate motifs, able to change their coordination due to external stimuli (such as the application of a sufficient voltage to oxidize or reduce the metal center) are good candidates for this purpose. Different coordination environments produce different molecular properties, which allow the retention of information. Furthermore, in order to become good memory devices, those changes must be reversible. A wide number of ruthenium complexes containing sulfoxide ligands capable of carrying out linkage isomerism have been reported,[2] where their dynamic behavior is based on the higher affinity of Ru(II) and Ru(III) for S and O atoms, respectively, in agreement with hard−soft acid−base (HSAB)-Pearson theory.[3] Another interesting example of Ru complexes containing the ambidentate ligand 1-[6-(2,2′-bipyridyl)]-1-(2-pyridyl)ethanol (bpy-py-OH) (Chart 1) has been recently described by Johansson and Lomoth[4] and exhibits fast electron-transfer-induced linkage isomerization.

During the last three decades, Ru−aqua/oxo polypyridyl complexes have been used as oxidation catalysts due to their capacity to reach a wide range of oxidation states in a narrow potential range.[5] The simultaneous proton and electron removal (PCET) allows increasing the metal oxidation state at relatively low potentials.[6]

Chart 1. Drawing of the Ligands Discussed in This Work

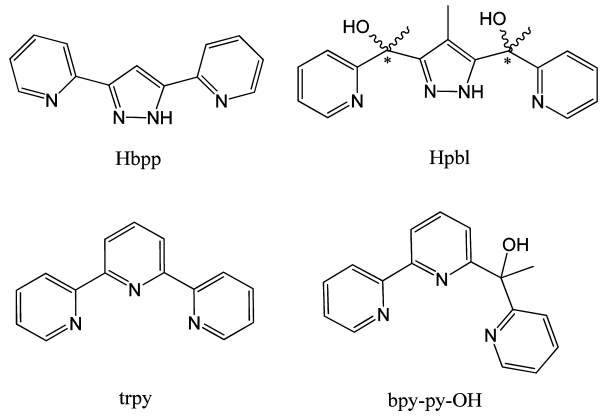

Over the past few years, our group has focused its attention on the understanding and mastering of metal cooperation in chemical reactions using dinuclear metal-aqua/oxo complexes.[7] For this purpose, the tetraaza dinucleating ligand 3,5-bis(2-pyridyl)pyrazole [Hbpp, Chart 1] has been used as bridging ligand between two Ru metal centers, and its catalytic properties have been established for oxidative transformations

Received: April 17, 2014
Published: July 22, 2014

   dx.doi.org/10.1021/ic5009076 | *Inorg. Chem.* 2014, 53, 8025−8035

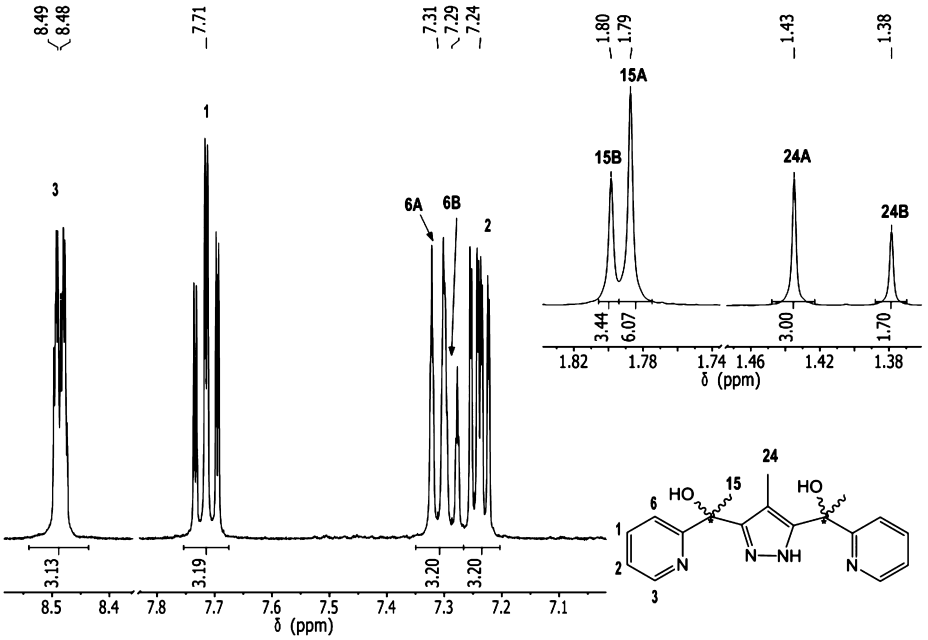

Figure 1. ^{1}H NMR spectrum of Hpbl in acetonitrile-d_3. Bottom: Aromatic region and numbering scheme. Top: Aliphatic region where a 3.0:1.7 diasteriomeric mixture ratio can be clearly observed for the Me protons.

such as water oxidation and alkene epoxidation.[8] When these Ru−aqua/oxo polypyridyl species are involved in catalytic oxidative transformations, the metal center cycles typically within oxidation states II−V.[9,10] The stabilization of all the oxidation states involved is of paramount importance in order to guarantee low kinetic barriers and thus catalyst viability.

Here on we report a new tetradentate bridging ligand, 1,1′-(4-methyl-1*H*-pyrazole-3,5-diyl)bis(1-(pyridin-2-yl)ethanol (Hpbl, Chart 1), potentially able to stabilize low and high oxidation states by adapting to the electronic demands of the metal center via linkage isomerism. In addition we also report two mononuclear Ru complexes containing this ligand of general formula $[RuX(Hpbl)(trpy)]^{y+}$ (X = Cl, y = 1; X = H_2O, y = 2) and their linkage isomerization capacities.

EXPERIMENTAL SECTION

Materials. All reagents used in the present work were obtained from Sigma-Aldrich Chemical Co. and were used without further purification. Reagent grade organic solvents were obtained from SDS. $RuCl_3{\cdot}3H_2O$ was supplied by Alfa Aesar and was used as received.

Preparations. The starting complex $[RuCl_3(trpy)]$[11] and 1′-(4-methyl-1*H*-pyrazole-3,5-diyl)diethanone[12] were prepared as previously described in the literature. All synthetic manipulations were routinely performed under nitrogen atmosphere using Schlenck tubes and vacuum line techniques.

1,1′-(4-Methyl-1H-pyrazole-3,5-diyl)bis(1-(pyridin-2-yl)ethanol) (Hpbl·1.5H$_2$O). A sample of 0.91 mL (9.39 mmol) of 2-bromopyridine was dissolved in 100 mL of dry THF with vigorous stirring at −78 °C. Then 6.2 mL of *n*-BuLi in hexane (1.6 M) was added drop by drop. After stirring the mixture for 30 min, 0.5 g (3.01 mmol) of 1′-(4-methyl-1*H*-pyrazole-3,5-diyl)diethanone dissolved in 20 mL of dry THF was added slowly with a syringe pump. The resulting mixture was stirred for 2 h at −78 °C and then warmed to 0 °C, acidified with a 10% HCl aqueous solution, and finally neutralized (until pH = 7) with a 10% K_2CO_3 aqueous solution. During this process the color of the solution changed from brown to yellow and finally to orange. The resulting mixture was warmed and extracted with $CHCl_3$ (3 × 100 mL) until the extracted organic phase was colorless. The collected organic phases were mixed, dried with anhydrous Na_2SO_4, and evaporated until a brown oil appeared. The oil was then purified by column chromatography using silica gel as stationary phase and ethyl acetate as eluent, giving the desired product in the fourth fraction as a 3.0:1.7 mixture of two diastereomers. Yield: 344 mg (35%). ^{1}H NMR (360 MHz, acetonitrile-d_3) δ 8 0.49 (ddd, 2H$_{3A}$, $^{3}J_{3-2}$ = 4.9 Hz, $^{4}J_{3-1}$ = 1.7 Hz, $^{5}J_{3-6}$ = 1.0 Hz), 8.48 (ddd, 2H$_{3B}$, $^{3}J_{3-2}$ = 4.9 Hz, $^{4}J_{3-1}$ = 1.7 Hz, $^{5}J_{3-6}$ = 1.0 Hz), 7.72 (ddd, 2H$_{1A,B}$, $^{3}J_{1-6}$ = 8.0 Hz, $^{3}J_{1-2}$ = 7.5 Hz, $^{4}J_{1-3}$ = 1.7 Hz), 7.31 (dt, 2H$_{6A}$, $^{3}J_{6-1}$ = 8.0 Hz, $^{4}J_{6-2,3}$= 1.3 Hz), 7.28 (dt, 2H$_{6B}$, $^{3}J_{6-1}$ = 8.0 Hz, $^{4}J_{6-2,3}$ = 1,0 Hz), 7.24 (ddd, 2H$_{2B}$, $^{3}J_{2-1}$ = 7.5 Hz, $^{3}J_{2-3}$ = 4.9 Hz, $^{4}J_{2-6}$ = 1.0 Hz), 7.24 (ddd, 2H$_{2A}$, $^{3}J_{2-1}$ = 7.5 Hz, $^{3}J_{2-3}$ = 4.9 Hz, $^{4}J_{2-6}$ = 1.0 Hz), 5.23 (s, 2H$_{14B}$), 5.21 (s, 2H$_{14A}$), 1.79 (s, 6H$_{15B}$), 1.78 (s, 6H$_{15A}$), 1.43 (s, 3H$_{24A}$), 1.37 (s, 3H$_{24B}$). ^{13}C{^{1}H} NMR (100 MHz, acetonitrile-d_3) δ 164.9 (C$_{5A}$), 164.8 (C$_{5B}$), 148.4 (C$_{3A}$), 148.3 (C$_{3B}$), 138.1 (C$_{1B}$), 138.1 (C$_{1A}$), 123.2 (C$_{2A,B}$), 121.0 (C$_{6A,B}$), 110.5 (C$_{17B}$), 110.3 (C$_{17A}$), 73.9 (C$_{13A}$), 73.8 (C$_{13B}$), 29.3 (C$_{15B}$), 29.3 (C$_{15A}$), 9.0 (C$_{24A}$), 9.0 (C$_{24B}$). ^{15}N NMR, projection from HMBC experiment (600 MHz, acetone-d_6): δ 298.7 (N$_{4-8}$). ESI-MS (MeOH): m/z 324.1, 347.1 (M + Na). Anal. Calcd (%) for ($C_{18}H_{23}N_4O_{3.5}$): C, 61.52; H, 6.59; N, 15.94. Found: C, 61.78; H, 6.36; N, 15.80. The NMR labels are keyed in Figure 1.

[Ru^{II}Cl(Hpbl)(trpy)](PF$_6$)·C$_3$H$_6$O·0.5H$_2$O, 1(PF$_6$) C$_3$H$_6$O·0.5H$_2$O. A sample of 400 mg (0.908 mmol) of $[RuCl_3(trpy)]$ and 77 mg (1.816 mmol) of LiCl were dissolved in 40 mL of dry MeOH containing 250 μL (1.816 mmol) of NEt_3. The mixture was stirred at room temperature (RT) for 20 min, and then 294 mg (0.908 mmol) of Hpbl was added. The resulting solution was stirred at 40 °C overnight. After that, the mixture was filtered, and 2 mL of a saturated aqueous NH_4PF_6 solution and 5 mL of water were added. The volume of the resulting solution was reduced on a rotary evaporator until a precipitate appeared. After 1 day at 5 °C the precipitate was filtered off. The solid was extracted with CH_2Cl_2 until the organic solvent was colorless, and the insoluble material was filtered off and discarded. The resulting solution was purified by column chromatography using neutral alumina as solid phase. The first three fractions eluted with a CH_2Cl_2/MeOH (140:1) mixture were discarded. The desired product was finally eluted with pure MeOH. This fraction was reduced to dryness, the brown powder obtained was dissolved in acetone, and again 1 mL of a saturated aqueous NH_4PF_6 solution and 3 mL of water were added. The volume was then reduced on a rotary evaporator until a solid came out. The mixture was then cooled in a refrigerator for 12 h, and the solid obtained was filtered off, washed with cold water (3 × 5 mL) and diethyl ether (3 × 5 mL), and vacuum-dried. The isolated product maintains the 3.0:1.7 diasteriomeric mixture of the

dx.doi.org/10.1021/ic5009076 | Inorg. Chem. 2014, 53, 8025−8035

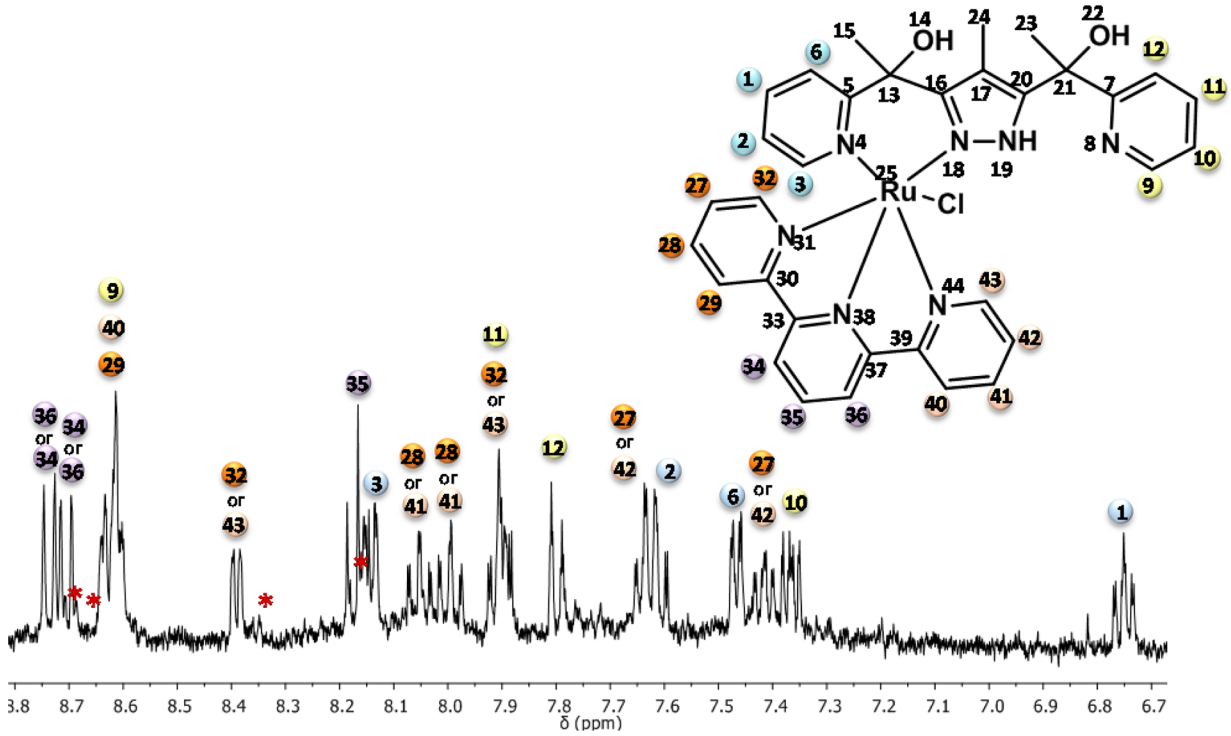

Figure 2. ^{1}H NMR spectrum of the aromatic region of a diastereomerically enriched mixture (8:1) of $\mathbf{1}^{+}$ and its corresponding drawing and numbering scheme. Orange and light orange trpy protons remain indistinguishable. The residual signals of low concentration diastereomer B are marked with a red asterisk.

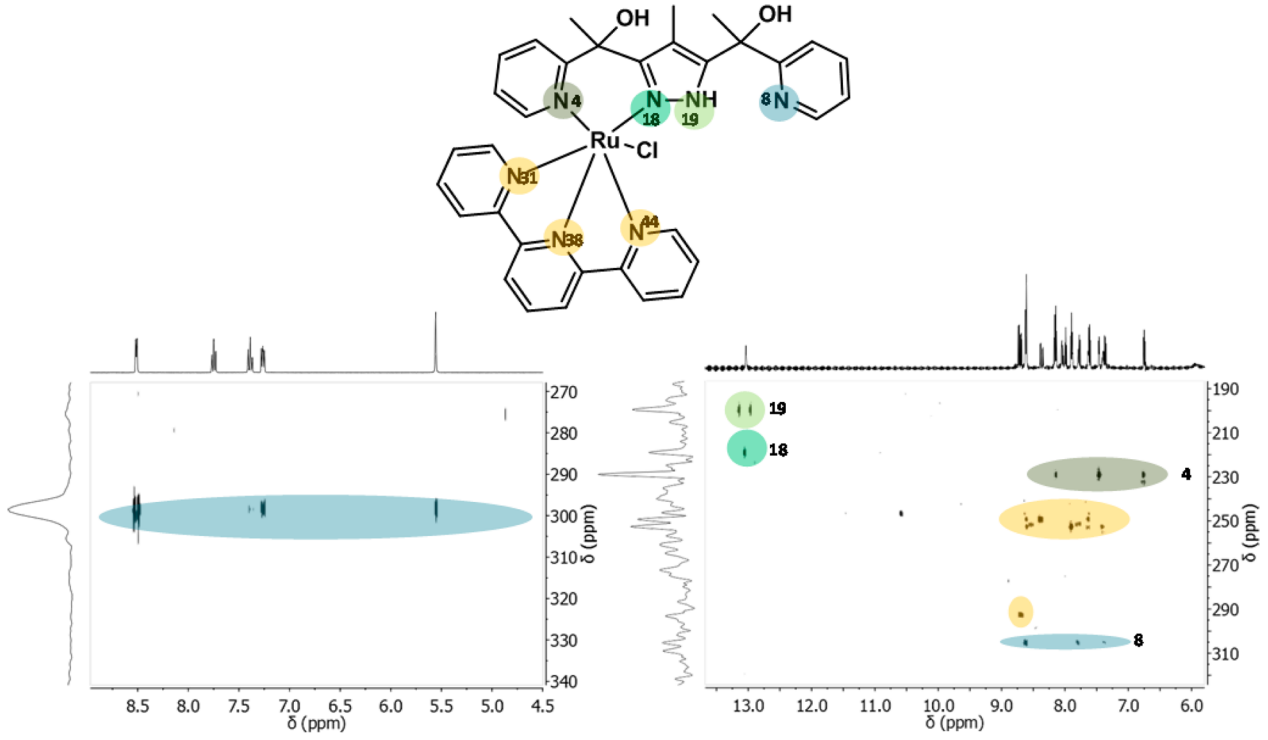

Figure 3. HMBC-N spectra for the Hpbl free ligand (left) and complex $\mathbf{1}^{+}$ (right) in acetone-d_6 together with a drawing and numbering scheme.

starting Hpbl ligand. Yield: 311 mg (41%). Anal. Calcd (%) for $C_{36}H_{38}ClF_6N_7O_{3.5}PRu$: C, 47.71; H, 4.23; N, 10.82. Found: C, 47.70; H, 4.26; N, 10.99. ^{1}H NMR (600 MHz, acetone-d_6): δ 8.73 (dd, $1H_{34A\text{ or }36A}$, $^{3}J_{34-35}$ = 8.1 Hz, $^{4}J_{34-36}$ = 0.6 Hz), 8.73 (dd, $1H_{34B\text{ or }36B}$, $^{3}J_{34-35}$ = 8.1 Hz, $^{4}J_{34-36}$ = 0.6 Hz), 8.71 (dd, $1H_{36A\text{ or }34A}$, $^{3}J_{36-35}$ = 8.1 Hz, $^{4}J_{36-34}$ = 0.6 Hz), 8.70 (dd, $1H_{36B\text{ or }34B}$, $^{3}J_{36-35}$ = 8.1 Hz, $^{4}J_{36-34}$ = 0.6 Hz), 8.64−8.60 (m, $3H_{29-40-9A,B}$), 8.39 (dd, $1H_{43A\text{ or }32A}$, $^{3}J_{43-42}$ = 5.4 Hz, $^{4}J_{43-41}$ = 1.6 Hz, $^{5}J_{43-40}$ = 0.6 Hz), 8.35 (dd, $1H_{43B\text{ or }32A}$, $^{3}J_{43-42}$ = 5.4 Hz, $^{4}J_{43-41}$ = 1.6 Hz, $^{5}J_{43-40}$ = 0.6 Hz), 8.16 (t, $1H_{35A}$, $^{3}J_{35-34,36}$ = 8.1 Hz), 8.15 (t, $1H_{35B}$, $^{3}J_{35-34,36}$ = 8.1 Hz), 8.14 (ddd, $1H_{3A,B}$, $^{3}J_{3-2}$ = 8.1 Hz, $^{4}J_{3-1}$ = 1.5 Hz, $^{5}J_{3-6}$ = 0.5 Hz), 8.05 (ddd, $1H_{41A\text{ or }28A}$, $^{3}J_{41-40}$ = 8.1 Hz, $^{3}J_{41-42}$ = 7.7 Hz, $^{4}J_{41-43}$ = 1.6 Hz), 8.04 (ddd, $1H_{41B\text{ or }28B}$, $^{3}J_{41-40}$ = 8.1 Hz,

dx.doi.org/10.1021/ic5009076 | Inorg. Chem. 2014, 53, 8025−8035

$^3J_{41-42}$ = 7.7 Hz, $^4J_{41-43}$ = 1.6 Hz), 8.00 (ddd, $1H_{28A,B\ or\ 41A,B}$, $^3J_{28-29}$ = 8.1 Hz, $^3J_{28-27}$ = 7.6 Hz, $^4J_{28-32}$ = 1.4 Hz), 7.90 (ddd, $1H_{11B}$, $^3J_{11-12}$ = 8.1 Hz, $^2J_{11-10}$ = 7.6 Hz, $^3J_{11-9}$= 1.8 Hz), 7.90 (ddd, $1H_{11A}$, $^3J_{11-12}$ = 8.1 Hz, $^2J_{11-10}$ = 7.6 Hz, $^3J_{11-9}$ = 1.8 Hz), 7.89 (d, $1H_{32A,B\ or\ 43A,B}$, under another signal), 7.79 (ddd, $1H_{12A}$, $^3J_{12-11}$ = 8.1 Hz, $^4J_{12-10}$ = 1.0 Hz, $^5J_{12-9}$ = 0.9 Hz), 7.77 (ddd, $1H_{12B}$, $^3J_{12-11}$ = 8.1 Hz, $^4J_{12-10}$ = 1.0 Hz, $^5J_{12-9}$ = 0.9 Hz), 7.63 (ddd, $1H_{42A\ or\ 27A}$, $^3J_{42-41}$ = 7.7 Hz, $^3J_{42-43}$ = 5.4 Hz, $^4J_{42-40}$ = 1.6 Hz), 7.62 (ddd, $1H_{42B\ or\ 27B}$, $^3J_{42-41}$ = 7.7 Hz, $^3J_{42-43}$ = 5.4 Hz, $^4J_{42-40}$ = 1.6 Hz), 7.61 (ddd $1H_{2A,B}$, $^3J_{2-3}$ = 8.1 Hz, $^3J_{2-1}$ = 7.2 Hz, $^4J_{2-6}$ = 1.6 Hz), 7.47 (ddd, $1H_{6A}$, $^3J_{6-1}$ = 6.1 Hz, $^4J_{6-2}$ = 1.6 Hz, $^5J_{6-3}$ = 0.5 Hz), 7.46 (ddd, $1H_{6B}$, $^3J_{6-1}$ = 6.1 Hz, $^4J_{6-2}$ = 1.6 Hz, $^5J_{6-3}$ = 0.5 Hz), 7.41 (ddd, $1H_{27A,B\ or\ 42A,B}$, $^3J_{27-28}$ = 7.6 Hz, $^3J_{27-32}$ = 5.7 Hz, $^4J_{27-32}$ = 1.5 Hz), 7.36 (ddd, $1H_{10A,B}$, $^3J_{10-11}$ = 7.6 Hz, $^3J_{10-9}$ = 4.8 Hz, $^4J_{10-12}$ = 1.0 Hz), 6.75 (ddd, $1H_{1A}$, $^3J_{1-2}$ = 7.2 Hz, $^3J_{1-6}$ = 6.1 Hz, $^4J_{1-3}$ = 1.5 Hz), 6.75 (ddd, $1H_{1A}$, $^3J_{1-2}$ = 7.2 Hz, $^3J_{1-6}$ = 6.1 Hz, $^4J_{1-3}$ = 1.5 Hz), 5.99 (s, $1H_{14\ or\ 22A,B}$), 5.91 (s, $1H_{14\ or\ 22A,B}$), 2.48 (s, $3H_{24B}$), 2.41 (s, $3H_{24A}$), 1.71 (s, $3H_{15B}$), 1.71 (s, $3H_{15A}$). $^{13}C\{^1H\}$ NMR (100 MHz, acetone-d_6): δ 171.3 ($C_{5A,B}$), 164.3 (C_{7A}), 164.2 (C_{7B}), 161.2 ($C_{33A,B}$ or $C_{37A,B}$), 161.1 ($C_{37A,B}$ or $C_{33A,B}$), 160.8 (C_{39A} or.C_{30B}), 160.8 (C_{39A} or.C_{30A}), 160.5 (C_{30B} or C_{39B}), 160.5 (C_{30A} or C_{39A}), 154.6 ($C_{43A,B}$ or $C_{32A,B}$), 153.88 (C_{6A}), 153.84 (C_{6B}), 153.0 (C_{32A} or C_{43A}), 153.0 (C_{32B} or C_{43B}), 152.8 ($C_{16A,B}$), 149.2 ($C_{29A,B}$ or $C_{40A,B}$), 148.9 ($C_{20A,B}$), 138.2 ($C_{11A,B}$), 137.8 (C_{41A} or C_{28A}), 137.8 (C_{41B} or C_{28B}), 137.77 (C_{28A} or C_{41A}), 137.75 (C_{28B} or C_{41B}), 137.56 (C_{2A}), 137.54 (C_{2B}), 134.37 (C_{35A}), 134.33 (C_{35B}), 128.18 (C_{42A} or C_{27A}), 128.16 (C_{42B} or C_{27B}), 128.06 (C_{27A} or C_{42A}), 128.04 (C_{27B} or C_{42B}), 125.21 (C_{3B}), 125.15 (C_{3A}), 124.6 ($C_{43A,B}$ or $C_{32A,B}$), 124.5 ($C_{1A,B}$), 124.4 (C_{9A}), 124.3 (C_{9B}), 123.74 ($C_{34A,B}$ or $C_{36A,B}$), 123.70 (C_{10B}), 123.66 (C_{10A}), 123.25 (C_{36A} or C_{34A}), 123.22 (C_{36B} or C_{34B}), 121.09 (C_{12B}), 121.04 (C_{12A}), 114.1 (C_{17A}), 113.8 (C_{17B}), 76.86 (C_{13} or C_{21A}), 76.76 (C_{13} or C_{21B}), 36.44 (C_{15A}), 36.38 (C_{15B}), 10.73 (C_{24B}), 10.68 (C_{24A}). ^{15}N NMR, projection from HMBC experiment (600 MHz, acetone-d_6): δ 199.6 (N_{19}, $^1J_{N-H}$ = 108.2 Hz), 219.1 (N_{18}), 228.9 (N_4), 249.3 (N_{44} or N_{31}), 252.6 (N_{31} or N_{44}), 292.2 (N_{38}), 305.2 (N_8). ESI-MS (MeOH): m/z 694.1 ($[M - PF_6^-]^+$). UV−vis (CH_2Cl_2) [λ_{max}, nm (ε, M^{-1} cm^{-1})]: 274 (5217), 317 (1523), 390 (1335), 487 (1278), 519 (1127), 615 (377). CV (DCM/TBAH): $E_{1/2}$ = 0.86 V. NMR labels for complexes $\mathbf{1}^+$ and $\mathbf{2}^{2+}$ are keyed in Figures 2 and 3.

$[Ru^{II}(Hpbl)(trpy)(H_2O)]^{2+}$, $\mathbf{2}^{2+}$. This complex was quantitatively generated in situ by dissolving 8.4 mg (1 mmol) of complex $\mathbf{1}(PF_6)$ into 10 mL of 0.1 M triflic acid aqueous solution (pH = 1). ^1H NMR (400 MHz, acetone-d_6/D_2O/CF_3SO_3D): δ 8.93 (d, $1H_{9A,B}$, $^3J_{9-10}$ = 5.8 Hz), 8.77 (td, $1H_{11B}$, $^3J_{11-10,12}$ = 8.1 Hz, $^4J_{11-9}$ = 1.6 Hz), 8.76 (td, $1H_{11A}$, $^3J_{11-10,12}$ = 8.1 Hz, $^4J_{11-9}$ = 1.6 Hz), 8.66 (d, $1H_{34A\ or\ 36A}$, $^3J_{34-35}$ = 8.1 Hz), 8.64 (d, $1H_{34B\ or\ 36B}$, $^3J_{34-35}$ = 8.1 Hz), 8.60 (d, $1H_{34B\ or\ 36B}$, $^3J_{36-35}$ = 8.1 Hz), 8.60 (d, $1H_{34A\ or\ 36A}$, $^3J_{36-35}$ = 8.05 Hz), 8.53 (d, $1H_{32A,B\ or\ 43A,B}$, $^3J_{32-27}$ = 8.0 Hz), 8.51 (d, $1H_{43A,B\ or\ 32A,B}$, $^3J_{43-42}$ = 8.0 Hz), 8.36 (d, $1H_{29B\ or\ 40B}$, $^3J_{29-28}$ = 5.7 Hz), 8.31 (d, $1H_{12B}$, $^3J_{12-11}$ = 8.1 Hz), 8.30 (d, $1H_{12A}$, $^3J_{12-11}$ = 8.1 Hz), 8.27 (d, $1H_{29A\ or\ 40A}$, $^3J_{29-28}$ = 5.7 Hz), 8.16 (ddd, $1H_{10A,B}$, $^3J_{10-11}$ = 8.1 Hz, $^3J_{10-9}$ = 5.8 Hz, $^4J_{10-12}$ = 1.1 Hz), 8.12 (t, $1H_{35A}$, $^3J_{35-34,36}$ = 8.1 Hz), 8.12 (t, $1H_{35B}$, $^3J_{35-34,36}$ = 8.1 Hz), 8.09 (dd, $1H_{40A,B\ or\ 29A,B}$, $^3J_{40-41}$ = 5.7 Hz, $^4J_{40-42}$= 1.4 Hz), 8.00 (dd, $1H_{3A,B}$, $^3J_{3-2}$ = 8.0 Hz, $^4J_{3-1}$ = 1.4 Hz), 7.95 (ddd, $1H_{27A,B\ or\ 42A,B}$, $^3J_{27-32}$ = 8.0 Hz, $^3J_{27-28}$ = 7.0 Hz, $^4J_{27-29}$ = 1.5 Hz), 7.93 (td, $1H_{42A,\ or\ 27A}$, $^3J_{42-41,43}$ = 8.0 Hz, $^4J_{42-40}$ = 1.4 Hz), 7.91 (td, $1H_{42B\ or\ 27B}$, $^3J_{42-41,43}$ = 8.0 Hz, $^4J_{42-40}$ = 1.40 Hz), 7.57 (ddd, $1H_{28B\ or\ 41B}$, $^3J_{28-27}$ = 7.0 Hz, $^3J_{28-29}$ = 5.7 Hz, $^4J_{28-32}$ = 1.2 Hz), 7.55 (ddd, $1H_{28A\ or\ 41A}$, $^3J_{28-27}$ = 7.0 Hz, $^3J_{28-29}$ = 5.7 Hz, $^4J_{28-32}$ = 1.2 Hz), 7.53 (ddd, $1H_{2A,B}$, $^3J_{2-3}$ = 8.0 Hz, $^3J_{2-1}$ = 7.4 Hz, $^4J_{2-6}$ = 1.5 Hz), 7.38 (ddd, $1H_{41A\ or\ 28A}$, $^3J_{41-42}$ = 8.0 Hz, $^3J_{41-40}$ = 5.7 Hz, $^4J_{41-43}$ = 1.1 Hz), 7.34 (d, $1H_{6A,B}$, $^3J_{6-1}$ = 6.0 Hz), 7.33 (ddd, $1H_{41B\ or\ 28B}$, $^3J_{41-42}$ = 8.0 Hz, $^3J_{41-40}$ = 5.7 Hz, $^4J_{41-43}$ = 1.1 Hz), 6.66 (ddd, $1H_{1A,B}$, $^3J_{1-2}$ = 7.4 Hz, $^3J_{1-6}$ = 6.0 Hz, $^4J_{1-3}$ = 1.4 Hz), 2.28 (s, $3H_{24B}$), 2.21 (s, $3H_{24A}$), 2.21 (s, $3H_{15B}$), 2.20 (s, $3H_{15A}$), 1.59 (s, $3H_{23B}$), 1.56 (s, $3H_{23A}$). $^{13}C\{^1H\}$ NMR (100 MHz, acetone-d_6/D_2O/CF_3SO_3D): δ 170.64 (C_{5B}), 170.59 (C_{5A}), 160.6 ($C_{33A,B}$ or $C_{37A,B}$), 160.5 ($C_{33A,B}$ or $C_{37A,B}$), 160.2 ($C_{30A,B}$), 159.7 ($C_{30A,B}$), 157.9 ($C_{7A,B}$), 154.7 ($C_{29A,B}$ or $C_{40A,B}$), 153.6 (C_{40B} or C_{29B}), 153.44 ($C_{40A\ or\ 29A\text{-}6A}$), 153.40 ($C_{6B}$), 148.80 ($C_{11B}$), 148.75 ($C_{11A}$), 144.2 ($C_{16A,B}$), 142.332 ($C_{9A}$), 142.29 ($C_{9B}$), 137.97 ($C_{42B}$ or C_{27B}), 137.95 (C_{42A} or C_{27A}), 137.88 (C_{27B} or C_{42B}), 137.82 (C_{27A} or C_{42A}), 137.56 (C_{2A}), 137.53 (C_{2B}), 135.0 ($C_{35A,B}$), 128.2 ($C_{20A,B}$), 128.2 (C_{41A} or C_{28A}), 128.2 (C_{41B} or C_{28B}), 128.0 ($C_{28A,B}$ or $C_{41A,B}$), 127.5 ($C_{10A,B}$), 125.6 (C_{12A}), 125.5 (C_{12B}), 124.9 (C_{3B}), 124.8 (C_{3A}), 124.5 (C_{1A}), 124.4 (C_{1B}), 124.3−124.2 ($C_{32A,B\ or\ 43A,B\text{-}3A,B}$), 123.7 ($C_{34B}$ or C_{36B}), 123.6 (C_{34A} or C_{36A}), 123.1 ($C_{34A,B}$ or $C_{36A,B}$), 115.5 (C_{17A}), 115.3 (C_{17B}), 76.3 (C_{13B} or C_{21B}), 76.2 (C_{13A} or C_{21A}), 71.5 (C_{13B} or C_{21B}), 71.3 (C_{13A} or C_{21A}), 36.0 (C_{23B}), 36.9 (C_{23A}), 27.2 (C_{15B}), 27.1 (C_{15A}), 10.2 (C_{24B}), 10.1 (C_{24A}). ^{15}N NMR, projection from HMBC experiment (600 MHz, acetone-d_6/D_2O/CF_3SO_3D): δ 289.0 (N_{38}), 250.4 (N_{44} or N_{31}), 247.2 (N_{44} or N_{31}), 225.9 (N_4), 196.6 (N_8). ESI-MS (MeOH): m/z 658.2 ($[M - 2PF_6^- - H^+]^+$). UV−vis (pH = 1, 0.1 M triflic acid aqueous solution) [λ_{max}, nm (ε, M^{-1} cm^{-1})]: 270 (5504), 310 (5449), 360 (1461), 450 (1207), 480 (1170). CV (pH = 1.0 triflic acid aqueous solution): $E_{1/2}$ = 0.72 V, $E_{1/2}$ = 0.93 V.

Instrumentation and Measurements. UV−vis spectroscopy was performed with an HP8453 spectrometer using 1 cm quartz cells. ^1H NMR spectroscopy was performed on a Bruker DPX 360, 400, and 600 MHz at the Universitat Autònoma de Barcelona magnetic resonance service (SeRMN-UAB). Samples were run in acetone-d_6, acetonitrile-d_3, and D_2O with CF_3SO_3D or with NaOD with internal references (residual protons and/or tetramethylsilane). Elemental analyses were performed using a Carlo Erba CHMS EA-1108 instrument provided by the Chemical Analysis Service at UAB. ESI-MS experiments were performed on an HP298s GC-MS system from the CAS-UAB. Cyclic voltammetry (CV) experiments were performed with a PAR283 potentiostat using a three-electrode cell. A glassy carbon disk (3 mm diameter) was used as working electrode, platinum wire was used as auxiliary electrode, and a saturated sodium calomel electrode (SSCE) was used as the reference electrode. For the solutions of complexes in organic solvents, n-Bu_4NPF_6 was used as supporting electrolyte to yield a solution with a 0.1 M ionic strength. All $E_{1/2}$ values reported here were estimated from cyclic voltammetry as the average of the oxidative and reductive peak potentials $(E_{p,a} + E_{p,c})/2$ and are referred to the SSCE reference electrode. Species concentration was approximately 1 mM. For the construction of the Pourbaix diagram the following buffers were used: hydrogen phthalate/triflic acid up to pH = 4, hydrogen phthalate/sodium hydroxide for pH = 5.0, dihydrogen phosphate/sodium hydroxide for pH = 6.0, borax/triflic acid for pH = 7.0, hydrogen phosphate/sodium hydroxide for the pH range 8−9. Also 0.1 M triflic acid was used for pH = 1.0.

X-ray Crystal Structure Determination. Crystals of complex $[Ru^{II}(OH)(pbl)(trpy)]$ were obtained by slow evaporation of a $\mathbf{2}^{2+}$ D_2O/acetone-d_6/NaOD mixture. The measured crystals were prepared under inert conditions immersed in perfluoropolyether as protecting oil for manipulation.

Data Collection. The crystal structure of complex [Ru(trpy)(pbl)(OH)] was obtained at room temperature (298(2) K) on a Bruker SMART APEX CCD diffractometer using graphite-monochromated Mo Kα radiation from an X-ray tube. Programs used: data collection SMART,[13] data reduction Bruker Saint+,[14] and absorption correction SADABS.[15]

Structure Solution and Refinement. The solution and refinement of the crystal structure of complex [Ru(OH)(pbl)(trpy)] was achieved using the SHELTL[16] program.

Computational Details. The density functional theory (DFT) calculations have been carried out with the hybrid B3PW91 density ruthenium functional,[17] as implemented in the Gaussian 09 package.[18] The atoms have been represented with the quasi-relativistic effective core pseudopotentials of the Stuttgart group and the associated basis sets augmented with a polarization function (α = 1.235).[19] The remaining atoms (carbon, oxygen, nitrogen, and hydrogen) have been represented with 6-31G(d,p) basis sets.[20] The B3PW91 geometry optimizations were performed without any symmetry constraints, and the nature of the extrema (local minima or transition states, TS) was checked by analytical frequency calculations. The energies given throughout the article are Gibbs free energies with the ZPE corrections (however, inclusion of the ZPE corrections does not significantly modify the results) and thermal corrections in the gas phase. The solvent

dx.doi.org/10.1021/ic5009076 | Inorg. Chem. 2014, 53, 8025−8035

effect was introduced by the polarizable continuum model (PCM),[21] implemented by Tomasi and co-workers via single-point calculations on the optimized gas-phase geometries using the M06 functional[22] and the cc-pVTZ basis set for C, O, N, and H.[23] The cavity is created via a series of overlapping spheres. On the other hand, for the aqueous solvation free energy of the protons released, we assumed the value of 262.5 kcal mol^{-1} from the literature.[24]

RESULTS AND DISCUSSION

1. Synthesis. The synthetic strategy followed to prepare the new Hpbl ligand is depicted in Scheme 1. It involves the double nucleophilic attack of a pyridine lithiate to the two ketone carbonyl groups of the pyrazolyl derivative I (Scheme 1),[11]

Scheme 1. Synthesis of the Hpbl Ligand

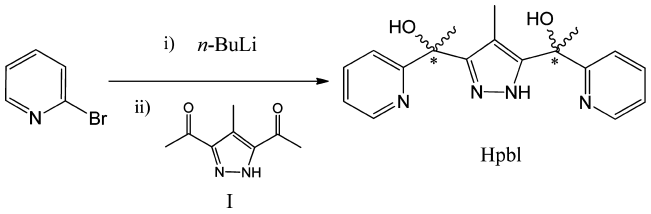

generating two alcoholic chiral centers. Column chromatography of the reaction crude gave, in the last eluted fraction, the desired Hpbl ligand as a mixture of two diastereomers in a ratio of 3.0:1.7, as can be observed in the ^{1}H NMR displayed in Figure 1.

The mononuclear chlorido complex $\mathbf{1}^+$ was obtained by the direct reaction of equimolar amounts of Hpbl and [$RuCl_3$(trpy)] in the presence of NEt_3 at 40 °C, as depicted in Scheme 2. Finally the aqua complex $\mathbf{2}^{2+}$ was quantitatively generated in situ when $\mathbf{1}^+$ was dissolved in acidic aqueous solutions. All the new compounds reported here were characterized by the usual analytic and spectroscopic techniques (see Supporting Information Figures S1−S16).

2. NMR and UV−vis Spectroscopy. 1D and 2D NMR spectroscopy was used to structurally characterize in solution the Hpbl ligand as well as complexes $\mathbf{1}^+$ and $\mathbf{2}^{2+}$ (see Figures 1 and 2, the Experimental Section, and Figures S1−S6 in the Supporting Information).

For the Hpbl ligand, all the resonances observed in the ^{1}H NMR spectra for the free ligand can be unambiguously assigned based on their integrals, symmetry, and multiplicity. In solution, the Hpbl ligand presents either C_2- or σ-symmetry depending on the diastereoisomer, that bisects the pyrazolyl group and interconverts each side of the ligand, thus becoming magnetically equivalent, as can be noted in Figure 1. In this figure the 3.0:1.7 ratio of the two diastereoisomers appearing as a duplicate can also be observed. Particularly interesting and useful is the HMBC-N NMR, which shows the presence of all the Hpbl nitrogen resonances at 298.7 ppm, strongly coupled to H2, H3, and the OH proton, as shown in Figure 3.

Complexes $\mathbf{1}^+$ and $\mathbf{2}^{2+}$ have no symmetry elements due to the coordination of the Ru metal center on one of the ligand sides, and thus all the resonances are now magnetically different. For complex $\mathbf{1}^+$ we managed to highly enrich one sample up to a 8.0:1.0 diastereomeric ratio by means of preparative TLC. A ^{1}H NMR spectrum of the latter with the assignment is shown in Figure 2, and an additional 2D spectrum is depicted in the Supporting Information Figure S3. There are a number of features related to the NMR spectra that are worth mentioning and that are useful for the structural characterization of this complex. First, both alcohol protons can be observed at low and similar chemical shifts (5.99 and 5.91 ppm), which is indicative that they are not coordinated to the metal center. Second, the absence of resonances in the 9−10 ppm region is indicative of the *in*-isomer,[26] where the Ru−Cl bond is directed toward the center of the Hbpl ligand, meaning that the chlorido ligand is *trans* to the pyridyl ligand. On the other hand the *out*-isomer that would have the Ru−Cl bond *trans* to the Ru−N pyrazolyl bond would be responsible for the deshielding of the H3 hydrogen toward the 9−10 ppm region.[26]

Third, the HMBC-N NMR shown in Figure 3 is fully consistent with the previous assignment. The pyrazolyl N atoms appear at 200 and 215 ppm for that coordinated to Ru and the protonated one, respectively. The former appears as a doublet due to its coupling with the proton. The noncoordinated pyridyl Hbpl N8 atom appears at 305 ppm, very close to the ones of the free ligands, while the coordinated N4 one is upfield shifted to 230 ppm. Finally the trpy N atoms appear very close at 249 and 251 ppm. It is interesting to see here that the HMBC-N NMR experiment is a very powerful tool for the diagnosis of coordinated versus noncoordinated N atoms of a particular ligand, especially with multiple N-coordinating sites.

The NMR spectra for the aqua complex $\mathbf{2}^{2+}$ was recorded in acetone-d_6 acidified with a drop of a 0.1 M solution of CF_3SO_3D in D_2O. The main differences in the spectra with regard to the $\mathbf{1}^+$ spectrum are the upfield shift of the resonances belonging to the noncoordinated pyridyl ligand that is protonated under these conditions. A spectacular effect is observed in the NMR when complex $\mathbf{2}^{2+}$ is recorded in basic

Scheme 2. Synthetic Strategy Used for the Preparation of the Complexes Described in This Work[a]

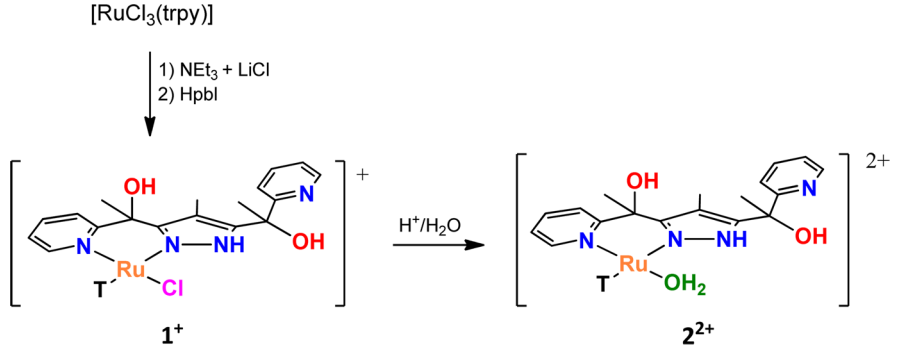

[a]T represents the trpy ligands where the axial N atoms are not shown for simplicity.

dx.doi.org/10.1021/ic5009076 | Inorg. Chem. 2014, 53, 8025−8035

solution (acetone-d_6 basified with a drop of 0.1 M NaOD in D_2O). Under these conditions a large amount of resonances appear that are indicative of new complexes being formed. DOSY experiments carried out under exactly the same conditions indicate that the new complexes formed are mononuclear in nature, since all of them have the same diffusion coefficients and similar to $[Ru(bpea)(bpy)(H_2O)]^{2+}$ (bpea is *N*,*N*-bis(pyridin-2-ylmethyl)ethanamine; bpy is 2,2′-bipyridine) used as reference[25,28a] (see Supporting Information, Figure S6).

The UV−vis spectra in CH_2Cl_2 and H_2O/trifluoroacetic acid for complexes $\mathbf{1}^+$ and $\mathbf{2}^{2+}$ are displayed in Figure 4 and Figures S8 and S9 in the Supporting Information. The observed absorptions agree with those reported for similar complexes.[26] The spectra can be divided in three different regions: between 200 and 350 nm, where very intense bands are observed due to intraligand $\pi-\pi^*$ transitions;[27] between 350 and 560 nm, in which there are mainly broad unsymmetrical Ru(dπ)-trpy/Hpbl(π^*) metal-to-ligand charge transfer (MLCT) bands;[28] and finally the region above 560 nm, in which d−d transitions are observed.[29] Figure S8 (Supporting Information) shows the UV−vis spectra for complexes $\mathbf{1}^+$ and $\mathbf{2}^{2+}$, where different band displacement for the broad overlapped Ru(dπ)-trpy/Hpbl(π^*) MLCT bands is observed. The blue-shift exhibited by complex $\mathbf{2}^{2+}$ confirms the coordination of the aqua ligand that relatively stabilizes the dπ(Ru) levels and therefore gives rise to more energetic electronic transitions.[28]

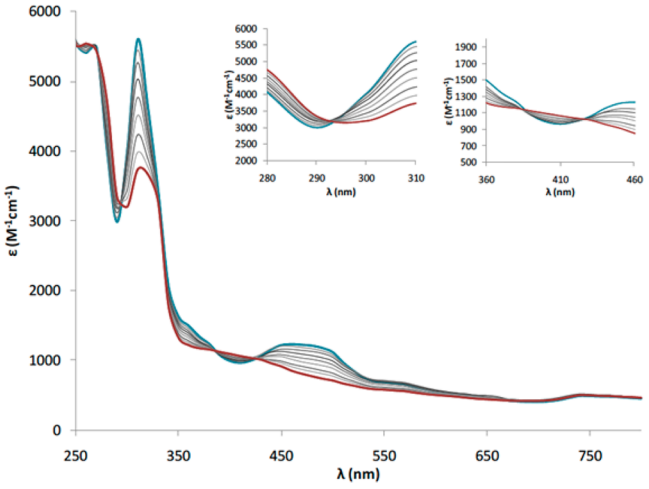

Figure 4. UV−vis spectrophotometric titration of complex $\mathbf{2}^{2+}$ with Ce(IV). A sample of 0.5 mL of $\mathbf{2}^{2+}$ 0.1 mM was titrated with eight sequential additions of 10 μL of 0.6 mM Ce(IV). Both solutions are in a pH = 1.0 trifluoroacetic acid aqueous solution. Ru(II): blue line, Ru(III): red line. Inset: Zoom of the isosbestic points region.

Generation of the higher oxidation state species of complex $\mathbf{2}^{2+}$ was followed spectrophotometrically. The spectrum obtained upon progressive addition of small amounts of Ce(IV) to an aqueous solution of the complex at pH = 1.0 until the addition of 1 oxidant equivalent is shown in Figure 4. The three isosbestic points observed at λ = 294, 386, and 426 nm suggest the neat generation of the Ru(III) species. Addition of a second equivalent of Ce(IV) produces a further oxidation of the complex, which generates the corresponding Ru(IV)-oxo species, which is almost featureless in the visible region, as has been described for analogous complexes.[30] This second redox process also takes place with the presence of isosbestic points at 294, 386, and 426 nm and is shown in the Supporting Information, Figure S9.

3. Electrochemistry and Linkage Isomerism. The redox properties of complexes $\mathbf{1}^+$ and $\mathbf{2}^{2+}$ have been studied by cyclic voltammetry using glassy carbon disk electrodes. A common feature to most Ru−aqua complexes is the fact that their redox waves are more diffuse than the ones for the Ru−Cl complexes, which are generally very well-defined. In order to improve this, we tried a variety of working electrodes including boron-doped diamond electrodes, Pt ore, and even Au electrodes, but they did not yield any significant improvement.

Complex $\mathbf{1}^+$, dissolved in dichloromethane and using 0.1 M *n*-Bu_4NPF_6 as supporting electrolyte, displays one electrochemically quasi-reversible redox wave (see Supporting Information Figure S10) at $E_{1/2}$ = 0.840 V, which is assigned to the formation of the corresponding Ru(III) complex.

$$\underset{\mathbf{1}^+}{[Ru^{II}Cl(Hpbl)(trpy)]^+} \rightarrow \underset{\mathbf{1}^{2+}}{[Ru^{III}Cl(Hpbl)(trpy)]^{2+}} + 1e^- \quad (1)$$

Complex $\mathbf{2}^{2+}$ was generated in situ by dissolving $\mathbf{1}^+$ in a 0.1 M trifluoroacetic acid (pH = 1.0) aqueous solution. At high scan rates (1 V/s) the CV of $\mathbf{2}^{2+}$ presents two different redox processes (Figure 5a), the first and more intense one at $E_{1/2}$ = 0.725 V, which is associated with the first one-electron oxidation (wave A in Figure 5a),

$$\underset{\mathbf{2}^{2+}}{[Ru^{II}(Hpbl)(trpy)(H_2O)]^{2+}} \rightarrow \underset{\mathbf{2}^{3+}}{[Ru^{III}(H_2O)(Hpbl)(trpy)]^{3+}} + 1e^- \quad (2)$$

and the second and weaker one at $E_{1/2}$ = 0.932 V corresponding to the III/IV oxidation step (wave B in Figure 5a),

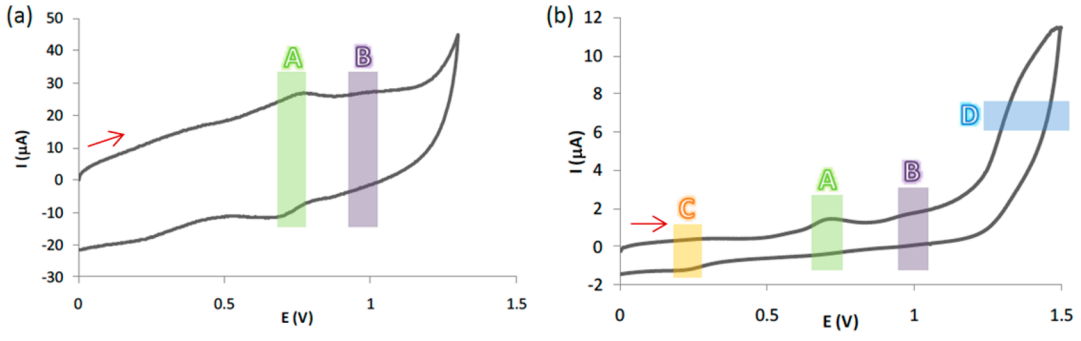

Figure 5. CV of complex $\mathbf{2}^{2+}$ at pH = 1.0 in a 0.1 M CF_3COOH aqueous solution at (a) 1 V/s and (b) 20 mV/s. The red arrow indicates the scanning direction.

dx.doi.org/10.1021/ic5009076 | Inorg. Chem. 2014, 53, 8025−8035

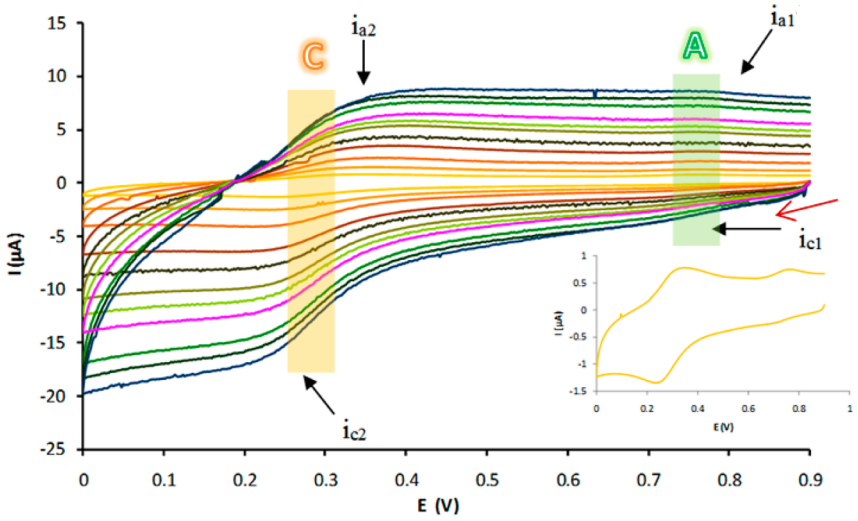

Figure 6. Cyclic voltammograms of complex $\mathbf{2}^{2+}$ in 0.1 M CF_3COOH aqueous solution at pH = 1.0, scanning cathodically, and applying an initial equilibration time of 3 min at 0.90 V. Scan rates: 20, 50, 100, 200, 300, 400, 500, 700, 800, 900, and 1000 mV/s. The red arrow indicates the scanning direction. i_{a1}: anodic peak intensity of the Ru(III/II)-N_5 process; i_{a2}: anodic peak intensity of the Ru(III/II)-ON_4 process; i_{c1}: cathodic peak intensity of the Ru(III/II)-N_5 process; i_{c1}: cathodic peak intensity of the Ru(III/II)-ON_4 process. Inset: CV at a scan rate of 20 mV/s.

$$\underset{\mathbf{2}^{3+}}{[Ru^{III}(H_2O)(Hpbl)(trpy)]^{3+}} \rightarrow \underset{\mathbf{2}^{3+}}{[Ru^{IV}(OH)(Hpbl)(trpy)]^{3+}} + 1e^- + 1H^+ \quad (3)$$

At a scan rate of 0.1 V/s and up to 1.5 V (Figure 5b) a large anodic current is observed (D in Figure 5b) that is associated with a further one-electron oxidation of the complex to Ru(V) with concomitant electrocatalytic oxygen generation similarly proposed for other mononuclear Ru−aqua complexes.[9a]

The presence of linkage isomerization is observed by CV when a solution of complex $\mathbf{2}^{2+}$ is scanned cathodically after holding an applied potential of 0.9 V for 3 min (see Figure 6) at different scan rates and observing the changes in $[i_{c1}]/[i_{a1}]$ and $[i_{c2}]/[i_{a2}]$ of the waves at 0.30 (wave C in Figure 6) and 0.8 V (wave A in Figure 6), respectively. The latter is the wave associated with the Ru(III/II) of complex $\mathbf{2}^{2+}$ labeled Ru-N_5 (the ruthenium metal center coordinated by five nitrogen atoms of the ligands: three from the trpy and two from the Hpbl) in Scheme 3, whereas the wave at 0.3 V is associated with the III/II couple for the Ru-ON_4(Pz) isomer (coordination to the ruthenium metal center by one hydroxyl oxygen and four nitrogen atoms: three from trpy and one from the pyrazolyl moiety of the Hpbl ligand; this isomer nomenclature is further described in Scheme 3 and Figure 9). It is proposed that when the oxidation state III for the Ru^{III}−N_5 ($\mathbf{2}^{3+}$) isomer is reached, the oxygen from the alkoxy is coordinated with concomitant decoordination of the pyridyl group of the Hpbl ligand, generating a new isomer labeled Ru^{III}-ON_4(Pz) ($\mathbf{2}^{3+}$). This hypothesis is further corroborated by the strong cathodic shift (roughly 500 mV) of the new couple due to strong sigma-donation capacity of the anionic alkoxy coordination and is in agreement with the HSAB-Pearson theory.[3] Further evidence for this coordination environment comes from the isolation of a low-quality crystal of Ru^{II}-ON_4(Pz) ($\mathbf{2}^{3+}$) (see Supporting Information Table S1 and Figure S7). Although distances and angles are not reliable for this structure, the connectivity among atoms is fully trustworthy and coincides with the proposed structure for the Ru^{II}-ON_4(Pz) ($\mathbf{2}^{3+}$) complex.

The complete thermodynamic cycle associated with this linkage isomerization is presented in Scheme 3. All the thermodynamic

Scheme 3. Thermodynamic Cycle for the Linkage Isomerization Process Taking Place upon the Electrochemical Oxidation of $\mathbf{2}^{2+}$ at pH = 1.0

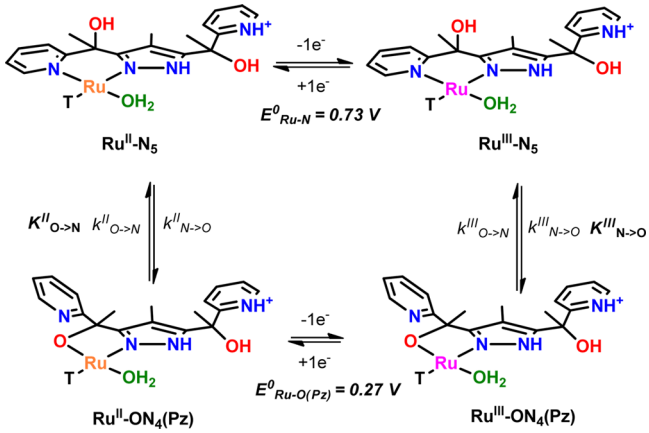

and kinetic parameters involved in this cycle can be potentially extracted experimentally from CV measurements as we and other have shown for related systems.[2,4] However, in the present case the intensities of the waves involved are weak and wide, and thus it is practically impossible to obtain reliable data. For this reason we have turned to DigiSim,[31] a CV simulation package, in order to computationally extract the mentioned thermodynamic and kinetic parameters (see Supporting Information Figure S17).

These parameters are presented in Table 1 together with those of related complexes, [Ru(bpy-py-OH)(4′-(pyrrolidin-1-yl)-2,2′:6′,2″-terpyridine)]$^{2+}$, $\mathbf{3}^{2+}$, and [Ru(bpy-py-OH)(4′-(*p*-tolyl)-2,2′:6′,2″-terpyridine)]$^{2+}$, $\mathbf{4}^{2+}$, previously reported in the literature, where the N → O linkage isomerization is also described for the bpy-py-OH ligand (see Chart 1 for a drawing). It is interesting to see that while the equilibrium constants $K^{II}_{O\rightarrow N} = 6.7 \times 10^6$ and $K^{III}_{N\rightarrow O} = 8.9$ are relatively similar, the kinetic rate constants are about 2 to 4 orders of magnitude smaller, manifesting the fact that this process is very slow for $\mathbf{2}^{2+}$. The latter could be ascribed to the Ru-N_5-H_2O nature of $\mathbf{2}^{2+}$, whereas the reported ones are based on Ru-N_6-type coordination.

dx.doi.org/10.1021/ic5009076 | *Inorg. Chem.* 2014, 53, 8025−8035

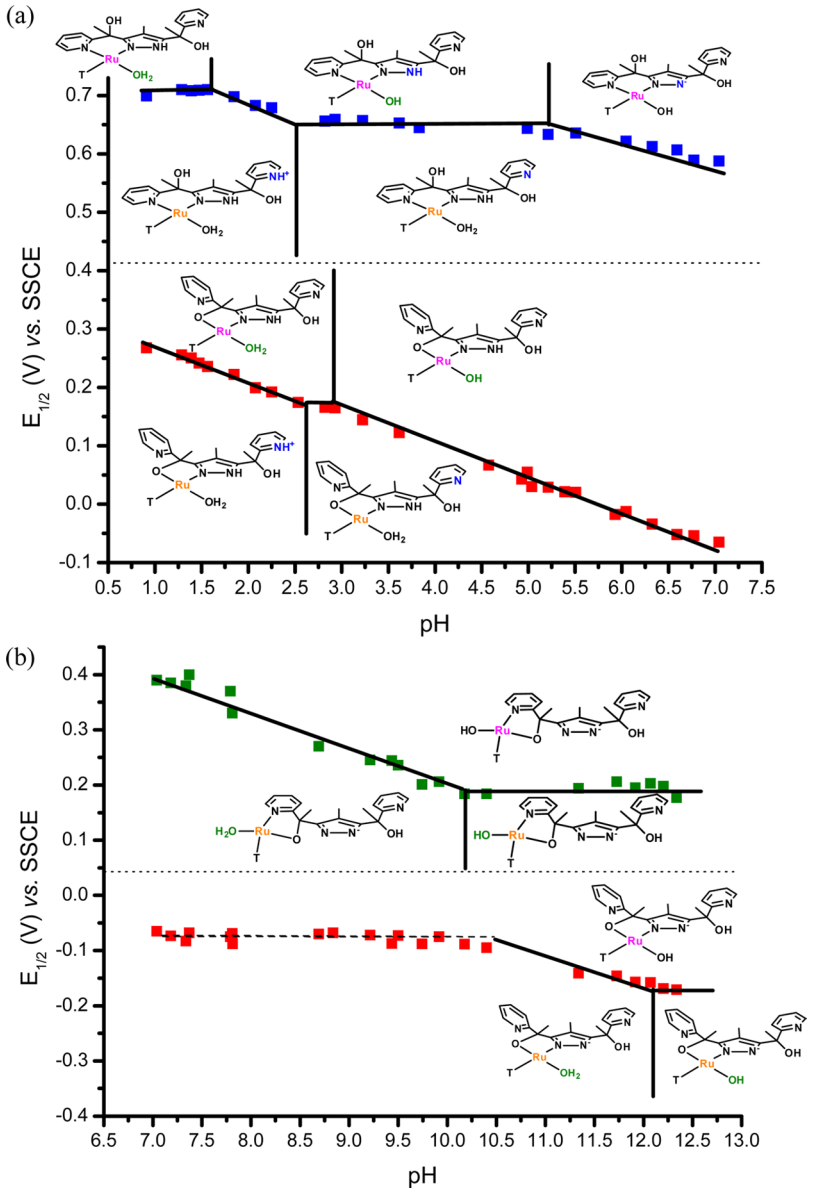

Figure 7. Pourbaix diagrams for the different isomers of complex $\mathbf{2}^{2+}$. (a) pH range 1−7, (b) pH range 7−12. The colored moiety is involved in the proton change. Color codes: Ru(III), pink; Ru(II), orange.

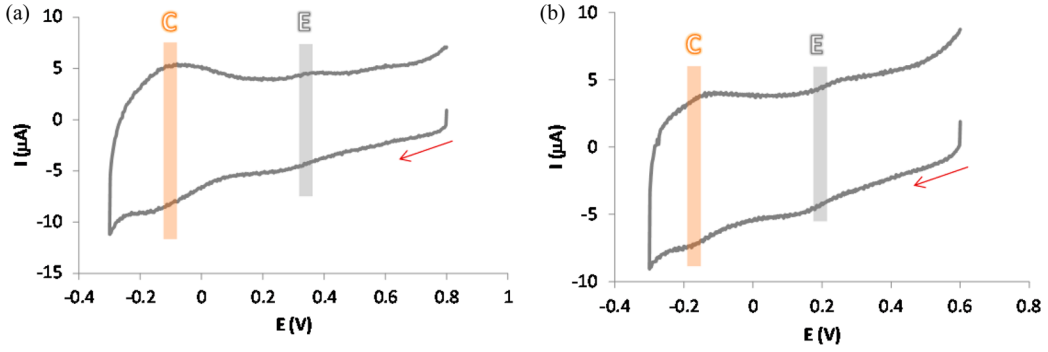

Figure 8. Cyclic voltammogram of complex $\mathbf{2}^{2+}$ at a scan rate of 100 mV/s scanning cathodically with 3 min equilibration time at (a) 0.80 V at pH = 8.0 and (b) 0.60 V at pH = 12.0. The red arrow indicates the scanning direction.

Experiments to determine the pH-dependence of the Ru(III/II) redox for $\mathbf{2}^{2+}$ from pH 0 to 7 have been carried out, and a corresponding Pourbaix diagram is presented in Figure 7a, where the different proton content of the dominant species is specified. The vertical lines indicate the pK_a's involved.

dx.doi.org/10.1021/ic5009076 | *Inorg. Chem.* 2014, 53, 8025−8035

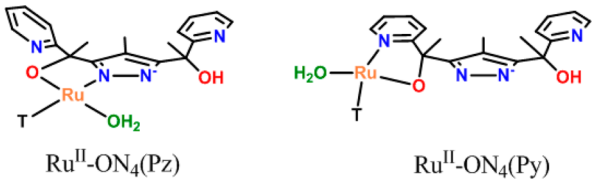

Figure 9. Drawing of the two coexisting isomers for complex 2^{2+} in the pH range 7−12.

Table 1. Thermodynamic and Kinetic Parameters for the Electrochemically Induced Linkage Isomerization of 2^{2+} and Related Systems[a]

	2^{2+}	3^{2+c}	4^{2+c}
$E_{1/2}$, N (V)[b]	0.73	0.755	0.972
$E_{1/2}$, O (V)[b]	0.27	0.305	0.465
$K^{II}_{O\rightarrow N}$	6.7×10^6	3.4×10^6	2.1×10^6
$K^{III}_{N\rightarrow O}$	8.9	12	200
$k^{II}_{O\rightarrow N}$ (s^{-1})	0.01	500	800
$k^{II}_{N\rightarrow O}$ (s^{-1})	7.4×10^{-7}	1.47×10^{-4}	3.81×10^{-4}
$k^{III}_{O\rightarrow N}$ (s^{-1})	0.03	1.25	1.25
$k^{III}_{N\rightarrow O}$ (s^{-1})	0.30	15	250

[a]Aqueous solution (pH = 1) at 298 K. [b]Potential referenced vs SSCE. [c]3^{2+} is [Ru(bpy-py-OH)(4′-(pyrrolidin-1-yl)-2,2′:6′,2″-terpyridine)]$^{2+}$, and 4^{2+} is [Ru(bpy-py-OH)(4′-(*p*-tolyl)-2,2′:6′,2″-terpyridine)]$^{2+}$, both described in ref 4a.

Above pH 7, and as previously shown in the NMR, new isomeric species are generated. A CV (Figure 8) at this pH region indicates that the Ru-ON_4(Pz) species still exists, as shown by the continuity of the III/II redox couple over pH, but a new set of waves at higher redox potentials appears (Figure 7b and Figure 8 wave E).

We associate this new waves with the Ru-ON_4(py) (2^{2+}) isomer (coordination to Ru through one hydroxyl oxygen and four nitrogen atoms: three from the trpy and one from the pyridyl group of Hpbl) depicted in the right-hand side of Figure 9, where the pyrazole N is exchanged by the pyridyl ring maintaining the alkoxy coordination.

The assignment is consistent with the monomeric nature obtained from the DOSY NMR experiment and the increased redox potential with regard to the Ru-ON_4(Pz) isomer, due to the replacement of the anionic pyrazolate moiety by a neutral pyridyl coordinating group from the same Hpbl ligand. In Table 2 are gathered selected thermodynamic parameters for all the complexes described in the present work together with those of related complexes reported in the literature for purposes of comparison.

The different geometries and relative stability among the linkage isomers of 2^{2+} at pH = 4.0 and at oxidation states II and III have been further analyzed by means of DFT calculations. For Ru(II) (Figure 10, top) the Ru^{II}-N_5 coordination environment is clearly favored, in agreement with the HSAB-Pearson theory,[3] with the corresponding Ru^{II}-ON_4(Pz) and Ru^{II}-ON_4(Py) linkage isomers 24.6 and 21.7 kcal mol^{-1} higher in energy, respectively. At oxidation state III (Figure 5, bottom) the Ru^{III}-ON_4(Pz) and Ru^{III}-ON_4(Py) species are thermodynamically favored versus Ru^{III}-N_5 by 0.5 and 5.9 kcal mol^{-1}, respectively, also in agreement with the HSAB-Pearson theory, although now the relative energies are much closer to one another. The higher relative stability of the Ru^{II}-ON_4(Py) species with respect to the Ru^{II}-N_4(Pz) one is due to the *cis* geometrical disposition of the Ru−O moieties as well as the rather strong H-bond between a hydrogen atom of the aquo ligand and the oxygen of the Ru−O moiety in *cis* (2.070 Å). While the Ru^{III}-ON_4(Py) is the most thermodynamically favored at this oxidation state and pH according to DFT, TS energies might be responsible for the generation of the Ru^{III}-ON_4(Pz) isomer, which is the experimentally observed species. This is important to underline here since, as mentioned at the beginning of this section, the linkage isomerization processes observed here are very slow. A full set of coordinates and absolute energies (in au) for all the DFT-optimized complexes are presented in the Supporting Information (Table S2).

Table 2. Electrochemical Data (pH = 1.0) for the ru−aqua Complexes Described in this Work and Others for Purposes of Comparison

entry	complex[a]	$E_{1/2}$(III/II)[b]	$E_{1/2}$(IV/III)[b]	ΔE[d]	ref
1	$[Ru^{II}(N_5)H_2O]^{2+}$, 2^{2+}	0.72	0.93	210	[e]
2	$[Ru^{II}(trpy)(bpy)OH_2]^{2+}$	0.81	1.10	290	5e
3	*in*-$[Ru^{II}(Hbpp)(trpy)OH_2]^{2+}$	0.66			2f
4	$[Ru^{II}(ON_4(Pz))H_2O]^{2+}$	0.24			[e]
5	$\{[Ru^{II}(trpy)(H_2O)]_2(\mu\text{-dcpz})]\}^{+}$	0.20			7a
6	$[Ru^{II}(ON_4(Py))H_2O]^{2+c}$	0.38			[e]
7	*cis*-$[Ru^{II}(trpy)(pic)OH_2]^{+c}$	0.38	0.56	180	29b

[a]Ligand abbreviations used: trpy = 2,2′:6′,2″-terpyridine, bpy = 2,2′-bipyridine, Hbpp = 3,5-bis(2-pyridyl)pyrazole, pic = picolinate, dcpz = pyrazole-3,5-dicarboxylate ligand. [b]Redox potentials in volts are reported with regard to the SSCE reference electrode. [c]Measured at pH = 7 (phosphate buffer). [d]$\Delta E = E_{1/2}(IV/III) - E_{1/2}(III/II)$ in mV. [e]This work.

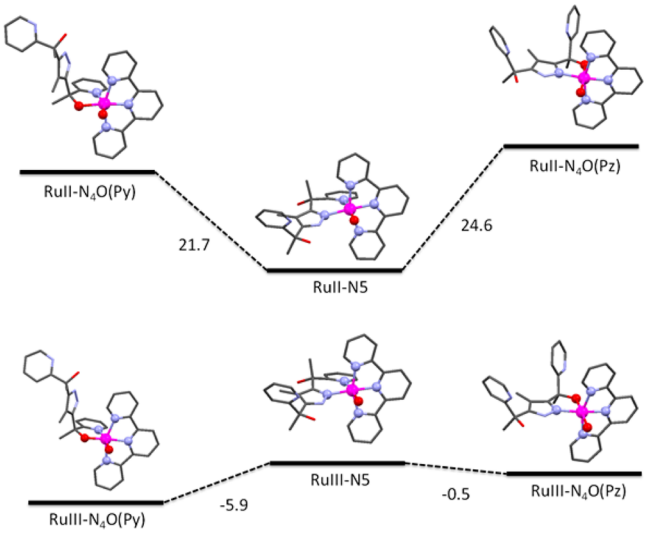

Figure 10. Relative energy diagram for the DFT-optimized geometries of the cationic moieties of the linkage isomers of 2^{2+} at pH = 4.0: Ru(II) (top) and Ru(III) (bottom). Energies are given in kcal mol^{-1}. Color codes: Ru, magenta; O, red; N, blue; C, gray (H atoms are omitted for the sake of clarity).

CONCLUSIONS

A new tetradentate ditopic ligand, Hpbl, with multiple N- and O-coordination sites has been prepared and fully characterized. The ligand is designed so that N- or O-coordination can be chosen depending of the nature and the oxidation state of the metal used. Mononuclear Ru−Cl, 1^{+}, and Ru−aqua, 2^{2+}, complexes have been prepared and spectroscopic and electrochemically characterized. Both complexes contain the tridentate

dx.doi.org/10.1021/ic5009076 | Inorg. Chem. 2014, 53, 8025−8035

meridional trpy ligand together with Hpbl completing the expected octahedral coordination. Given the multiple coordination sites of the Hpbl ligand, NMR has been crucial to fully characterize the structure of the complexes in solution at oxidation state II. Furthermore, the HMBC-N NMR experiment has been proven to be a very powerful tool for the diagnosis of coordinated versus noncoordinated N atoms for Hpbl, which can be obviously extended to related complexes where this might be needed.

The existence of linkage isomerization fostered by the oxidation of Ru(II) to Ru(III) in $\mathbf{2}^{2+}$ has been clearly shown by CV, and the thermodynamic and kinetic parameters related to the thermodynamic cycle have been extracted using DigiSim, an electrochemistry simulation package. Here the alkoxo group replaces the initially coordinated pyridyl group generating the N → O isomerization that we labeled as $[Ru(N_5)(H_2O)]^{2+}$ to $[Ru(ON_4(Pz))(H_2O)]^{2+}$ (see Scheme 3). Electrochemistry and NMR also reveal the presence of a new isomer in basic solutions, where the pyrazolyl coordinating group is replaced by the pyridyl group, thus forming $[Ru(ON_4(Py))(H_2O)]^{2+}$, as indicated in Figure 9. Finally geometrical optimizations have also been carried out by means of DFT calculations, which provide further support for all the isomers observed experimentally.

■ ASSOCIATED CONTENT

Supporting Information

Computational details and further spectroscopic (1D and 2D NMR) and electrochemical measurements for the reported complexes. This material is available free of charge via the Internet at http://pubs.acs.org.

■ AUTHOR INFORMATION

Corresponding Authors

*E-mail: xavier.sala@uab.cat.
*E-mail: lluis.escriche@uab.cat.
*E-mail: allobet@iciq.es.

Notes

The authors declare no competing financial interest.

■ ACKNOWLEDGMENTS

Support from MINECO (CTQ2011-26440, CTQ-2013-49075-R, and CTQ2011-23156-C02-02) is gratefully acknowledged. L.F. is grateful for the award of a PIF doctoral grant from UAB. A.P. is grateful to the European Commission (CIG09-GA-2011-293900) and the Spanish MINECO (Ramón y Cajal contract RYC-2009-05226).

■ REFERENCES

(1) (a) Wagenknecht, P. S.; Ford, P. C. *Coord. Chem. Rev.* **2011**, *255*, 591−616. (b) Jurow, M.; Schuckman, A. E.; Batteas, J. D.; Drain, C. M. *Coord. Chem. Rev.* **2010**, *254*, 2297−2310. (c) Ceroni, P. *Electrochemistry of Functional Supramolecular Systems*; Wiley: Hoboken NJ, 2010. (d) De Salvo, B.; Molas, G.; Perniola, L.; Jahan, C.; Buckley, J.; Jalaguier, E.; Gely, M. In *ECS Transactions*; Vienna, Austria, 2009; pp 151−162. (e) Akita, M.; Koike, T. *Dalton Trans.* **2008**, 3523. (f) Nishihara, H.; Kanaizuka, K.; Nishimori, Y.; Yamanoi, Y. *Coord. Chem. Rev.* **2007**, *251*, 2674−2687. (g) Baranoff, E.; Collin, J.; Furusho, J.; Furusho, Y.; Laemmel, A.; Sauvage, J. *Inorg. Chem.* **2002**, *41*, 1215−1222. (h) Ballardini, R.; Balzani, V.; Credi, A.; Gandolfi, M. T.; Venturi, M. *Int. J. Photoenerg.* **2001**, *3*, 63−77. (i) Ashton, P. R.; Ballardini, R.; Balzani, V.; Credi, A.; Dress, K. R.; Ishow, E.; Kleverlaan, C. J.; Kocian, O.; Preece, J. A.; Spencer, N.; Stoddart, J. F.; Venturi, M.; Wenger, S. *Chem.—Eur. J.* **2000**, *6*, 3558−3574.

(2) (a) Roeser, S.; Maji, S.; Benet-Buchholz, J.; Pons, J.; Llobet, A. *Eur. J. Inorg. Chem.* **2013**, *2013*, 232−240. (b) Benet-Buchholz, J.; Comba, P.; Llobet, A.; Roeser, S.; Vadivelu, P.; Wiesner, S. *Dalton Trans.* **2010**, *39*, 3315−3320. (c) Hamaguchi, T.; Ujimoto, K.; Ando, I. *Inorg. Chem.* **2007**, *46*, 10455−10457. (d) Rachford, A. A.; Rack, J. J. *J. Am. Chem. Soc.* **2006**, *128*, 14318−14324. (e) Butcher, D. P.; Rachford, A. A.; Petersen, J. L.; Rack, J. J. *Inorg. Chem.* **2006**, *45*, 9178−9180. (f) Sens, C.; Rodríguez, M.; Romero, I.; Llobet, A.; Parella, T.; Sullivan, B. P.; Benet-Buchholz, J. *Inorg. Chem.* **2003**, *42*, 2040−2048. (g) Atolagbe, P. O.; Taylor, K. N.; Wood, S. E.; Rheingold, A. L.; Harper, L. K.; Bayse, C. A.; Brunker, T. J. *Inorg. Chem.* **2013**, *52*, 1170−1172.

(3) Pearson, R. G. *J. Am. Chem. Soc.* **1963**, *85*, 3533−3539.

(4) (a) Johansson, O.; Johannissen, L.; Lomoth, R. *Chem.—Eur. J.* **2009**, *15*, 1195−1204. (b) Johansson, O.; Lomoth, R. *Inorg. Chem.* **2008**, *47*, 5531−5533. (c) Johansson, O.; Lomoth, R. *Chem. Commun.* **2005**, 1578−1580.

(5) (a) Serrano, I.; López, M. I.; Ferrer, I.; Poater, A.; Parella, T.; Fontrodona, X.; Solà, M.; Llobet, A.; Rodríguez, M.; Romero, I. *Inorg. Chem.* **2011**, *50*, 6044−6054. (b) Prades, A.; Peris, E.; Albrecht, M. *Organometallics* **2011**, *30*, 1162−1167. (c) Roeser, S.; Farràs, P.; Bozoglian, F.; Martínez-Belmonte, M.; Benet-Buchholz, J.; Llobet, A. *ChemSusChem* **2011**, *4*, 197−207. (d) Tada, M.; Muratsugu, S.; Kinoshita, M.; Sasaki, T.; Iwasawa, Y. *J. Am. Chem. Soc.* **2010**, *132*, 713−724. (e) Dakkach, M.; López, M. I.; Romero, I.; Rodríguez, M.; Atlamsani, A.; Parella, T.; Fontrodona, X.; Llobet, A. *Inorg. Chem.* **2010**, *49*, 7072−7079. (f) Benet-Buchholz, J.; Comba, P.; Llobet, A.; Roeser, S.; Vadivelu, P.; Wiesner, S. *Dalton Trans.* **2010**, *39*, 3315. (g) Jiang, G.; Chen, J.; Thu, H.; Huang, J.; Zhu, N.; Che, C. *Angew. Chem., Int. Ed.* **2008**, *47*, 6638−6642. (h) Sala, X.; Santana, N.; Serrano, I.; Plantalech, E.; Romero, I.; Rodríguez, M.; Llobet, A.; Jansat, S.; Gómez, M.; Fontrodona, X.; Eur, J. *Inorg. Chem.* **2007**, 5207−5214. (i) Serrano, I.; Sala, X.; Plantalech, E.; Rodríguez, M.; Romero, I.; Jansat, S.; Gómez, M.; Parella, T.; Stoeckli-Evans, H.; Solans, X.; Font-Bardia, M.; Vidjayacoumar, B.; Llobet, A. *Inorg. Chem.* **2007**, *46*, 5381−5389. (j) Rodríguez, M.; Romero, I.; Sens, C.; Llobet, A. *J. Mol. Catal. A: Chem.* **2006**, *251*, 215−220. (k) Punniyamurthy, T.; Velusamy, S.; Iqbal, J. *Chem. Rev.* **2005**, *105*, 2329−2364. (l) Catalano, V. J.; Heck, R. A.; Immoos, C. E.; Öhman, A.; Hill, M. G. *Inorg. Chem.* **1998**, *37*, 2150−2157. (m) Sens, C.; Romero, I.; Rodríguez, M.; Llobet, A.; Parella, T.; Benet-Buchholz, J. *J. Am. Chem. Soc.* **2004**, *126*, 7798−7799. (n) Rodríguez, M. *Electrochim. Acta* **2003**, *48*, 1047−1054. (o) Marmion, M. E.; Takeuchi, K. J. *J. Am. Chem. Soc.* **1988**, *110*, 1472−1480. (p) Marmion, M. E.; Takeuchi, K. J. *J. Am. Chem. Soc.* **1986**, *108*, 510−511.

(6) (a) Meyer, T. J.; Huynh, M. H. V. *Inorg. Chem.* **2003**, *42*, 8140−8160. (b) Dovletoglou, A.; Adeyemi, S. A.; Meyer, T. J. *Inorg. Chem.* **1996**, *35*, 4120−4127. (c) Suen, H. F.; Wilson, S. W.; Pomerantz, M.; Walsh, J. L. *Inorg. Chem.* **1989**, *28*, 786−791. (d) Roecker, L.; Kutner, W.; Gilbert, J. A.; Simmons, M.; Murray, R. W.; Meyer, T. J. *Inorg. Chem.* **1985**, *24*, 3784−3791. (e) Takeuchi, K. J.; Thompson, M. S.; Pipes, D. W.; Meyer, T. J. *Inorg. Chem.* **1984**, *23*, 1845−1851. (f) Binstead, R. A.; Moyer, B. A.; Samuels, G. J.; Meyer, T. J. *J. Am. Chem. Soc.* **1981**, *103*, 2897−2899. (g) Moyer, B. A.; Meyer, T. J. *Inorg. Chem.* **1981**, *20*, 436−444. (h) Moyer, B. A.; Meyer, T. J. *J. Am. Chem. Soc.* **1978**, *100*, 3601−3603.

(7) (a) Di Giovanni, C.; Poater, A.; Benet-Buchholz, J.; Cavallo, L.; Solà, M.; Llobet, A. *Chem.—Eur. J.* **2014**, *20*, 3898−3902. (b) Di Giovanni, C.; Vaquer, L.; Sala, X.; Benet-Buchholz, J.; Llobet, A. *Inorg. Chem.* **2013**, *52*, 4335−4345.

(8) García-Antón, J.; Bofill, R.; Escriche, L.; Llobet, A.; Sala, X. *Eur. J. Inorg. Chem.* **2012**, 4775−4789 and references therein.

(9) (a) Concepcion, J. J.; Tsai, M.; Muckerman, J. T.; Meyer, T. J. *J. Am. Chem. Soc.* **2010**, *132*, 1545−1557. (b) Bozoglian, F.; Romain, S.; Ertem, M. Z.; Todorova, T. K.; Sens, C.; Mola, J.; Rodríguez, M.; Romero, I.; Benet-Buchholz, J.; Fontrodona, X.; Cramer, C. J.; Gagliardi, L.; Llobet, A. *J. Am. Chem. Soc.* **2009**, *131*, 15176−15187. (c) Cape, J. L.; Siems, W. F.; Hurst, J. K. *Inorg. Chem.* **2009**, *48*, 8729−8735. (d) Nunes, G.; Alexiou, A.; Toma, H. *J. Catal.* **2008**, *260*, 188−

192. (e) Cape, J. L.; Hurst, J. K. *J. Am. Chem. Soc.* **2008**, *130*, 827−829. (f) Hurst, J. *Coord. Chem. Rev.* **2005**, *249*, 313−328. (g) Bennett, S.; Brown, S. M.; Conole, G.; Kessler, M.; Rowling, S.; Sinn, E.; Woodward, S. *J. Chem. Soc., Dalton Trans.* **1995**, 367.
(10) (a) Francàs, L.; Sala, X.; Escudero-Adán, E.; Benet-Buchholz, J.; Escriche, L.; Llobet, A. *Inorg. Chem.* **2011**, *50*, 2771−2781. (b) Francàs, L.; Sala, X.; Benet-Buchholz, J.; Escriche, L.; Llobet, A. *ChemSusChem* **2009**, *2*, 321−329.
(11) Sullivan, B. P.; Calvert, J. M.; Meyer, T. J. *Inorg. Chem.* **1980**, *19*, 1404.
(12) (a) Sachse, A.; Penkova, L.; Noël, G.; Dechert, S.; Varzatskii, O.; Fritsky, I.; Meyer, F. *Synthesis* **2008**, 800−806. (b) Ghosh, A.; Bischoff, A.; Cappiello, J. *Eur. J. Org. Chem.* **2003**, 821−832. (c) Meth-Cohn, O.; Vuorinen, E.; Modro, T. A. *J. Org. Chem.* **1989**, *54*, 4822−4827. (d) Wulfman, D. *Tetrahedron* **1976**, *32*, 1257−1265.
(13) Data collection with *SMART*, Version 5.631; Bruker Advanced X-ray Solutions: Madison, WI, USA, 1997−2002.
(14) Data reduction with *SAINT+*, Version 6.36A; Bruker: Madison, WI, USA, 2001.
(15) *SADABS*, V.2.10 (2003); Bruker AXS Inc.: Madison, WI, USA, 2001. Blessing. *Acta Crystallogr.* **1995**, *A51*, 33−38.
(16) Structure solution and model refinement with *SHELXTL*, Version 6.14; Bruker AXS Inc.: Madison, WI, USA, 2000−2003.
(17) (a) Becke, A. D. *J. Chem. Phys.* **1993**, *98*, 5648−5652. (b) Perdew, J. P.; Wang, Y. *Phys. Rev. B* **1992**, *45*, 13244−13249.
(18) Frisch, M. J.; Trucks, G. W.; Schlegel, H. B.; Scuseria, G. E.; Robb, M. A.; Cheeseman, J. R.; Scalmani, G.; Barone, V.; Mennucci, B.; Petersson, G. A.; Nakatsuji, H.; Caricato, M.; Li, X.; Hratchian, H. P.; Izmaylov, A. F.; Bloino, J.; Zheng, G.; Sonnenberg, J. L.; Hada, M.; Ehara, M.; Toyota, K.; Fukuda, R.; Hasegawa, J.; Ishida, M.; Nakajima, T.; Honda, Y.; Kitao, O.; Nakai, H.; Vreven, T.; Montgomery, J. A., Jr.; Peralta, J. E.; Ogliaro, F.; Bearpark, M.; Heyd, J. J.; Brothers, E.; Kudin, K. N.; Staroverov, V. N.; Kobayashi, R.; Normand, J.; Raghavachari, K.; Rendell, A.; Burant, J. C.; Iyengar, S. S.; Tomasi, J.; Cossi, M.; Rega, N.; Millam, N. J.; Klene, M.; Knox, J. E.; Cross, J. B.; Bakken, V.; Adamo, C.; Jaramillo, J.; Gomperts, R.; Stratmann, R. E.; Yazyev, O.; Austin, A. J.; Cammi, R.; Pomelli, C.; Ochterski, J. W.; Martin, R. L.; Morokuma, K.; Zakrzewski, V. G.; Voth, G. A.; Salvador, P.; Dannenberg, J. J.; Dapprich, S.; Daniels, A. D.; Farkas, Ö.; Foresman, J. B.; Ortiz, J. V.; Cioslowski, J.; Fox, D. J. *Gaussian 09*, Revision D.01; Gaussian, Inc.: Wallingford, CT, 2009.
(19) (a) Andrae, D.; Haussermann, U.; Dolg, M.; Stoll, H.; Preuss, H. *Theor. Chim. Acta* **1990**, *77*, 123−141. (b) Bergner, A.; Dolg, M.; Kuchle, W.; Stoll, H.; Preuss, H. *Mol. Phys.* **1993**, *80*, 1431−1444.
(20) Hehre, W. J.; Ditchfield, R.; Pople, J. A. *J. Chem. Phys.* **1972**, *56*, 2257−2261.
(21) Barone, V.; Cossi, M. *J. Phys. Chem. A* **1998**, *102*, 1995−2001.
(22) Zhao, Y.; Truhlar, D. *Theor. Chem. Acc.* **2008**, *120*, 215−241.
(23) Dunning, T. H. *J. Chem. Phys.* **1989**, *90*, 1007−1023.
(24) Tawa, G. J.; Topol, I. A.; Burt, S. K.; Caldwell, R. A.; Rashin, A. A. *J. Chem. Phys.* **1998**, *109*, 4852−4963.
(25) Rodríguez, M.; Romero, I.; Sens, C.; Llobet, A.; Deronzier, A. *Electrochim. Acta* **2003**, *48*, 1047−1054.
(26) (a) Roeser, S.; Farràs, P.; Bozoglian, F.; Martínez-Belmonte, M.; Benet-Buchholz, J.; Llobet, A. *ChemSusChem* **2011**, *4*, 197−207. (b) Sens, C.; Rodríguez, M.; Romero, I.; Llobet, A.; Parella, T.; Benet-Buchholz, J. *Inorg. Chem.* **2003**, *42*, 8385−8394.
(27) (a) Hu, Y.-Z.; Xiang, Q.; Thummel, R. P. *Inorg. Chem.* **2002**, *41*, 3423−3428. (b) Brown, D.; Muranjan, S.; Jang, Y.; Thummel, R. *Org. Lett.* **2002**, *4*, 1253−1256. (c) Wu, F.; Thummel, R. P. *Inorg. Chim. Acta* **2002**, *327*, 26−30. (d) Juris, A.; Prodi, L.; Harriman, A.; Ziessel, R.; Hissler, M.; El-Ghayoury, A.; Wu, F.; Riesgo, E. C.; Thummel, R. P. *Inorg. Chem.* **2000**, *39*, 3590−3598. (e) Wu, F.; Riesgo, E. C.; Thummel, R. P.; Juris, A.; Hissler, M.; El-Ghayoury, A.; Ziessel, R. *Tetrahedron Lett.* **1999**, *40*, 7311−7314.
(28) (a) Rodríguez, M.; Romero, I.; Llobet, A.; Deronzier, A.; Biner, M.; Parella, T.; Stoeckli-Evans, H. *Inorg. Chem.* **2001**, *40*, 4150−4156. (b) Barkawi, K.; Llobet, A.; Meyer, T. J. *J. Am. Chem. Soc.* **1988**, *110*, 7751. (c) Llobet, A. *Inorg. Chim. Acta* **1994**, *221*, 125−131.
(29) (a) Haga, M.; Dodsworth, E. S.; Lever, A. B. P. *Inorg. Chem.* **1986**, *25*, 447−453. (b) Wong, C.-Y.; Che, C.-M.; Chan, M. C. W.; Leung, K.-H.; Phillips, D. L.; Zhu, N. *J. Am. Chem. Soc.* **2004**, *126*, 2501. (c) Kannan, S.; Ramesh, R.; Liu, Y. *J. Organomet. Chem.* **2007**, *692*, 3380. (d) Raja, N.; Ramesh, R. *Spectrochim. Acta Part A* **2010**, *75*, 713.
(30) (a) Takeuchi, K. J.; Thompson, M. S.; Pipes, D. W.; Meyer, T. J. *Inorg. Chem.* **1984**, *24*, 3784−3791. (b) Llobet, A.; Doppelt, P.; Meyer, T. J. *Inorg. Chem.* **1988**, *27*, 514−520. (c) Cheng, W. C.; Yu, W. Y.; Cheung, K. K.; Che, C. M. *J. Chem. Soc., Dalton Trans.* **1994**, 57−62.
(31) *DigiSim 3.03*, BASi DigiSim Simulation Software for Cyclic Voltammetry; BASi: West Lafayette, IN.